BREMSSTRAHLUNG DIODE PERFORMANCE ON MERCURY MIVA*

J.W. Schumer[ξ], R.J. Allen, R.J. Commisso, G. Cooperstein, D.D. Hinshelwood, D.P. Murphy, S.J. Stephanakis[t], S.B. Swanekamp[t], F.C. Young[t]

Plasma Physics Division, Naval Research Laboratory (Code 6770), 4555 Overlook Avenue SW, Washington, DC 20375 USA

Abstract

The Mercury generator is a ~6 MV, ~360 kA, ~50 ns magnetically-insulated voltage adder that recently became operational at the Naval Research Laboratory [1,2], providing a radiation environment of interest to both the DOE and DoD communities. To establish the bremsstrahlung dose and dose-rate production of Mercury, a series of large-area electron-beam (e-beam) diode experiments are performed in which the e-beam is deposited onto either a carbon or an optimized-thickness tantalum converter package. In this paper, experimental results are presented and compared with predictions from LSP (PIC) simulations [3] and ITS/Cyltran (Monte Carlo) calculations [4].

I. INTRODUCTION

To quantify the radiation environment of the Mercury generator, experiments are performed utilizing both carbon (C) and tantalum (Ta) converters. An array of CaF_2 thermoluminescent dosimeters (TLDs) and scintillator photodiodes (PDs) are used to measure the dose and dose-rate at various angles and distances from the source. For a particular bremsstrahlung converter package (including the anode foil, converter material, and electron beam stop), the voltage-dependent electron dynamics in the anode-cathode gap directly affect the magnitude and angular dependence of the radiation. A series of steady-state PIC simulations are performed using LSP [3] to model the electron distribution incident on the anode throughout the Mercury voltage pulse. These simulations include both power-flow electrons [5,6] born in the magnetically-insulated inductive voltage adder (MIVA) and electrons born in the diode. Electron scattering and energy loss in the bremsstrahlung converter package are modeled self-consistently by LSP. Predictions of the bremsstrahlung production (angular-dependent dose and dose-rate) are generated by using the PIC electron distributions as initial conditions for Monte Carlo radiation-transport simulations with the ITS-Cyltran code [4]. These predictions are compared with experiments on Mercury for both C and Ta converters, establishing the bremsstrahlung capabilities of the generator and benchmarking our predictive capability.

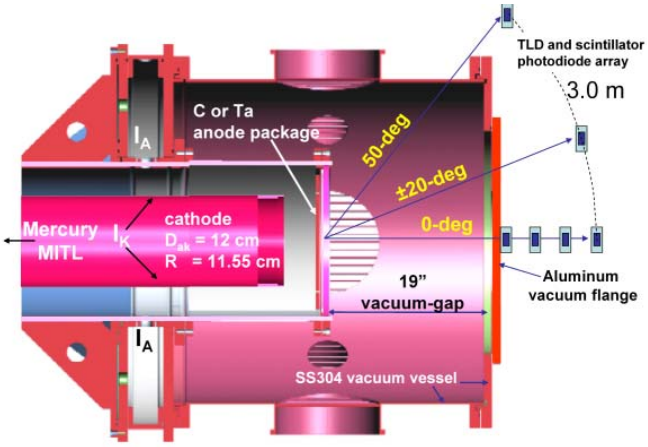

Figure 1. Schematic of the front-end of the Mercury pulsed power generator, showing current monitors, blade e-beam diode, vacuum vessel materials, and radiation diagnostics.

II. EXPERIMENTAL SET-UP

A schematic of the front-end of Mercury is shown in Fig. 1. The bremsstrahlung experiments described here use a cylindrical electron-beam diode in which high-energy electrons from a large-diameter, annular cathode impinge upon a planar anode. To minimize e-beam backscattering and subsequent ion formation, a low atomic-material was used as the anode ground plane. On Ta shots, an aluminum (Al) was used; for C shots, the carbon itself served this purpose. These designs inhibit pinching and result in an annular radiation source.

* Work supported by the Atomic Weapons Establishment (UK), Defense Threat Reduction Agency (U.S. DoD), and Sandia National Laboratories (U.S. DOE).

[t] Titan Corporation, Reston, VA 20190.

[ξ] email: schumer@nrl.navy.mil

Report Documentation Page

Form Approved
OMB No. 0704-0188

Public reporting burden for the collection of information is estimated to average 1 hour per response, including the time for reviewing instructions, searching existing data sources, gathering and maintaining the data needed, and completing and reviewing the collection of information. Send comments regarding this burden estimate or any other aspect of this collection of information, including suggestions for reducing this burden, to Washington Headquarters Services, Directorate for Information Operations and Reports, 1215 Jefferson Davis Highway, Suite 1204, Arlington VA 22202-4302. Respondents should be aware that notwithstanding any other provision of law, no person shall be subject to a penalty for failing to comply with a collection of information if it does not display a currently valid OMB control number.

1. REPORT DATE	2. REPORT TYPE	3. DATES COVERED
JUN 2005	**N/A**	**-**

4. TITLE AND SUBTITLE
Bremsstrahlung Diode Performance On Mercury Miva

5a. CONTRACT NUMBER
5b. GRANT NUMBER
5c. PROGRAM ELEMENT NUMBER

6. AUTHOR(S)

5d. PROJECT NUMBER
5e. TASK NUMBER
5f. WORK UNIT NUMBER

7. PERFORMING ORGANIZATION NAME(S) AND ADDRESS(ES)
Plasma Physics Division, Naval Research Laboratory (Code 6770), 4555 Overlook Avenue SW, Washington, DC 20375 USA

8. PERFORMING ORGANIZATION REPORT NUMBER

9. SPONSORING/MONITORING AGENCY NAME(S) AND ADDRESS(ES)

10. SPONSOR/MONITOR'S ACRONYM(S)
11. SPONSOR/MONITOR'S REPORT NUMBER(S)

12. DISTRIBUTION/AVAILABILITY STATEMENT
Approved for public release, distribution unlimited

13. SUPPLEMENTARY NOTES
See also ADM002371. 2013 IEEE Pulsed Power Conference, Digest of Technical Papers 1976-2013, and Abstracts of the 2013 IEEE International Conference on Plasma Science. IEEE International Pulsed Power Conference (19th). Held in San Francisco, CA on 16-21 June 2013., The original document contains color images.

14. ABSTRACT
The Mercury generator is a ~6 MV, ~360 kA, ~50 ns magnetically-insulated voltage adder that recently became operational at the Naval Research Laboratory [1,2], providing a radiation environment of interest to both the DOE and DoD communities. To establish the bremsstrahlung dose and dose-rate production of Mercury, a series of large-area electron-beam (e-beam) diode experiments are performed in which the e-beam is deposited onto either a carbon or an optimized-thickness tantalum converter package. In this paper, experimental results are presented and compared with predictions from LSP (PIC) simulations [3] and ITS/Cyltran (Monte Carlo) calculations [4].

15. SUBJECT TERMS

16. SECURITY CLASSIFICATION OF:			17. LIMITATION OF ABSTRACT	18. NUMBER OF PAGES	19a. NAME OF RESPONSIBLE PERSON
a. REPORT	b. ABSTRACT	c. THIS PAGE			
unclassified	**unclassified**	**unclassified**	**SAR**	**4**	

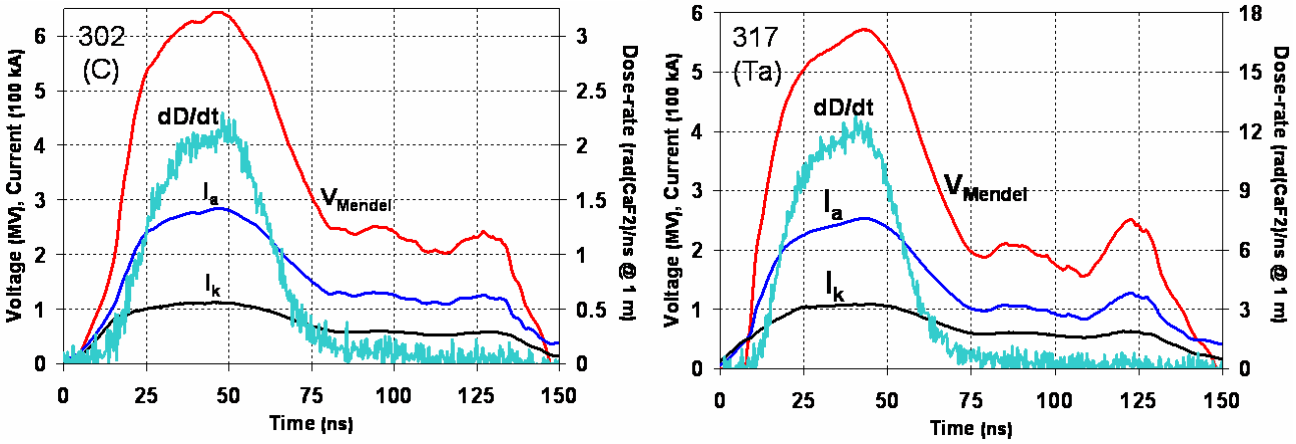

Figure 2. Anode and cathode currents measured near the diode on Shots 302 (carbon anode) and 317 (tantalum anode) are plotted versus time. The voltage is calculated using the Mendel formula, and peaks around 6 MV. Forward-directed dose-rates dD/dt are shown in units of [rad(CaF_2)/ns].

For Shots 280 – 306, a cylindrical-diode with an 11.55 cm radius cathode deposits an e-beam onto a 1.27-cm thick C anode, bolted onto a 2-cm thick Al beam stop. Throughout this shot series, the Marx charge and diode gap is varied from 50 to 75 kV and from 4 to 12 cm, respectively, to calibrate diagnostics and to study MITL powerflow and diode behavior [2,7]. A detailed analysis of Shot 302 is presented in this paper. The diode voltage on Shot 302 exceeds 6 MV and the MITL runs "line-limited" [7] with respect to the 12-cm A-K gap in the e-beam diode. The radiation production is also characterized with a full array of x-ray diagnostics.

For Shots 307 – 317, a cylindrical-diode with an 11.55 cm radius cathode deposits an e-beam onto a Ta converter package across a 12 cm gap. The Ta package consists of a thin anode Al foil (with aerodag), multiple foils of 25-μm Ta as the bremsstrahlung converter, and an Al beam stop. The material thicknesses are varied during this series to provide data for benchmarking to code predictions. Experiments and simulations at 6 MV suggest the on-axis dose is optimized for 75- to 100-μm of Ta. A detailed analysis of Shot 317 is presented in this paper. For this shot, the diode voltage is nearly 6 MV, the MITL flow is "line-limited" with respect to the 12-cm A-K gap, and the radiation production is characterized with a full array of x-ray diagnostics. For Shot 317, the Ta package consists of a 1.75-μm thick Al anode foil (with aerodag) and four 25-μm thick sheets of Ta, separated from a 2-cm thick Al beam stop by a 0.635-cm vacuum gap.

For Shots 302 (C) and 317 (Ta), the total thickness of the bremsstrahlung converter package is about twice the CSDA electron range at 6 MeV, primarily due to the 2-cm thick Al beam stop. The measured doses could be increased by reducing this beam-stop thickness.

To measure the dose and dose-rate during the experiments, an array of TLDs and PDs are located 3 m from the anode origin at 0°, ±20°, and 50° (see Fig. 1). Each PD consists of a 2.5-cm thick plastic scintillator (2-ns time response) coupled to a photodiode (0.5-ns rise time) and is mounted in a lead (Pb) shield to view the radiation source through a 1.3-cm diameter aperture. For Shot 317, a 1.905-cm thick Pb filter is used in front of the PDs to prevent saturation. Two TLDs are mounted approximately 2.54-cm from each of the PDs to measure the dose locally. The 1x1x6 mm CaF_2 TLDs are equilibrated with an Al cylinder of 4-mm wall thickness; this thickness is sufficient to isolate the TLDs from externally produced Compton electrons. The measured PD signals are scaled so that their time-integrals equal the dose measured by the co-located TLDs. Therefore, the PD-TLD configuration gives a time-resolved measure of dose-rate during the 50 ns pulse. Calculations shown below demonstrate that this approach is reasonably accurate.

II. EXPERIMENTAL RESULTS

Anode (I_a) and cathode (I_k) diode currents measured in Shots 302 and 317 are shown in Fig. 2. The current probe locations are indicated in Fig. 1. Because the diode impedance is large compared to the line-limited impedance of the MITL (Z_{diode} ~ 33 Ω > Z_{MITL} = 23 Ω), the Mendel voltage formula [8]

$$V = Z_o\sqrt{I_a^2 - I_k^2} - \frac{mc^2}{2e}\left(\frac{I_a^2}{I_k^2} - 1\right) \qquad (1)$$

is an accurate estimate of the diode voltage. In Eq. (1), the vacuum impedance Z_o = 30 Ω and mc^2/e = 511 kV. The calculated diode voltage V_{Mendel} peaks at approximately 6 MV for both shots. The measured anode currents and voltages are used in Eq. (3) below to calculate doses and dose-rates for comparison with measurements.

The on-axis dose at 1 m through 3.6 cm of Al (including the beam-stop) is about 87 rad(CaF_2) for Shot 302 and 445 rad(CaF_2) for Shot 317. The peak dose-rates are 2.1×10^9 rad(CaF_2)/sec in the 40-ns pulse for Shot 302 and 1.2×10^{10} rad(CaF_2)/sec in the 36-ns pulse for Shot 317. The measured on-axis dose-rates dD/dt, shown in

Fig. 2 with units of 10^9 rad(CaF_2)/sec, are accurately fit by 180 IV^2 for Shot 302 and 690 $IV^{2.5}$ for Shot 317, with currents in [A] and voltages in [MV].

III. MODELING

A series of steady-state LSP [3,5,6] simulations are performed at several voltages V_k to assess the radiation production from a given converter package, i.e. dose-efficiency $D(V_k,\theta)/Q$ as a function of V_k. *Dose-efficiency* is defined here as the dose D (energy absorbed per gram) per deposited electron charge Q in the bremsstrahlung diode. A symbolic representation of the algorithm used in this analysis is shown in Eq. (2).

$$V_k \underset{\text{LSP}}{\Rightarrow} f_e(x,p;V_k) \underset{\text{ITS}}{\Rightarrow} \gamma(\theta,E,Q;V_k) \underset{\mu(E)}{\Rightarrow} \frac{D}{Q}(\theta;V_k) \qquad (2)$$

PIC electrons incident on the anode are collected in each of these steady-state LSP simulations and are used to approximate the true electron distribution function (f_e) at a point in time during a 6-MV, 50-ns FWHM trapezoidal voltage pulse on Mercury. Each electron population collected is then passed into a 2d cylindrical Monte-Carlo electron/photon transport calculation using Cyltran [4]. This step accounts for internal absorption of bremsstrahlung photons and generates an angularly-dependent point-source spectrum $\gamma(\theta,E,Q)$ per incident electron charge Q. This spectrum is then used in conjunction with tabulated attenuation and absorption coefficients [NIST] to generate the dose-efficiency relations D/Q for each voltage, V_k, and angle, θ. These D/Q values from a series of steady-state voltage simulations ranging from 1 to 7 MV are fit with a power-law of the form αV^n and listed in Table 1.

To obtain an estimate of the dose, the appropriate D/Q power-law is integrated in time with the measured anode current

$$D(\theta) = \int I_a(t) \left(\frac{D}{Q}[V(t),\theta] \right) dt \qquad (3)$$

The estimated dose-rate is simply the integrand of Eq. (3), $dD/dt = I_a(t)\ (D/Q)$. The power-laws expressed in Table 1 are appropriate only for the experimental conditions modeled here; any change in MITL powerflow, diode configuration, converter material thicknesses, TLD equilibration, and photo-diode filtration will affect the results. However, these relations do suggest qualitatively how one might increase the dose by increasing the voltage and serve as a baseline for estimating the dose at any radial distance and angle from a point-source on this machine in this configuration.

Analysis of the PIC electrons and current contours indicate that the e-beam was incident on the converter package at an average angle of 20° to 30° near peak voltage. Qualitatively, the x-ray photographs (not shown here) indicate that the e-beam was azimuthally-uniform and justify the use of a cylindrical 2d model.

A comparison of measured and calculated doses and dose-rates is shown in Fig. 3. In the 0° and ±20° directions, simulations over-predict the dose by about 15%. On the other hand, predictions of dose-rates at 50° agree well with measurements. These comparisons suggest that the electron angles-of-incidence may not be modeled well. For Shot 317, the predicted curves agree with measurements during the rising portion of the radiation pulse but diverge later, suggesting that the voltage scaling changes in time.

Table 1. A comparison of measured and simulated dose-efficiency (D/Q) relations in units of [rad(CaF_2)/coulomb @ 1 m] as functions of voltage [MV] and at 0°, 20°, and 50°.

Shot#	D/Q	0°	20°	50°
302 (C)	Sim	190 $V^{2.09}$	158 $V^{2.23}$	15 $V^{2.75}$
	Exp	185 $V^{2.00}$	145 $V^{2.20}$	16 $V^{2.75}$
317 (Ta)	Sim	445 $V^{2.84}$	339 $V^{2.88}$	117 $V^{3.02}$
	Exp	690 $V^{2.5}$	450 $V^{2.7}$	145 $V^{2.9}$

IV. DISCUSSION

One potential source of error is the diode voltage; using Eq. (1) for voltage and an V^2 scaling for D/Q, a 5% error in measured current results in a 15% error in the predicted dose from Eq. (3). This emphasizes the importance of an independent measure of the voltage. Other sources of error include TLD calibration, room scatter, non-equilibrium electron incidence angles on the anode, and ion current in the diode; these will be considered in future work.

V. REFERENCES

[1] R.J. Commisso, et al., "Status of the Mercury Pulsed-Power Generator, a 6-MV, 360-kA, Magnetically-Insulated Inductive Voltage Adder," in Proc. 14th IEEE International Pulsed Power Conference (Dallas, TX, June 2003), p. 383.

[2] R.J. Allen, et al., "Initialization and Operation of Mercury, A 6-MV MIVA (Magnetically-Insulated Inductive Voltage Adder)," to be in Proc. 15th IEEE International Pulsed Power Conference (Monterey, CA, June 2005).

[3] D.V. Rose, et al., "Coupled particle-in-cell and Monte Carlo transport modeling of intense radiographic

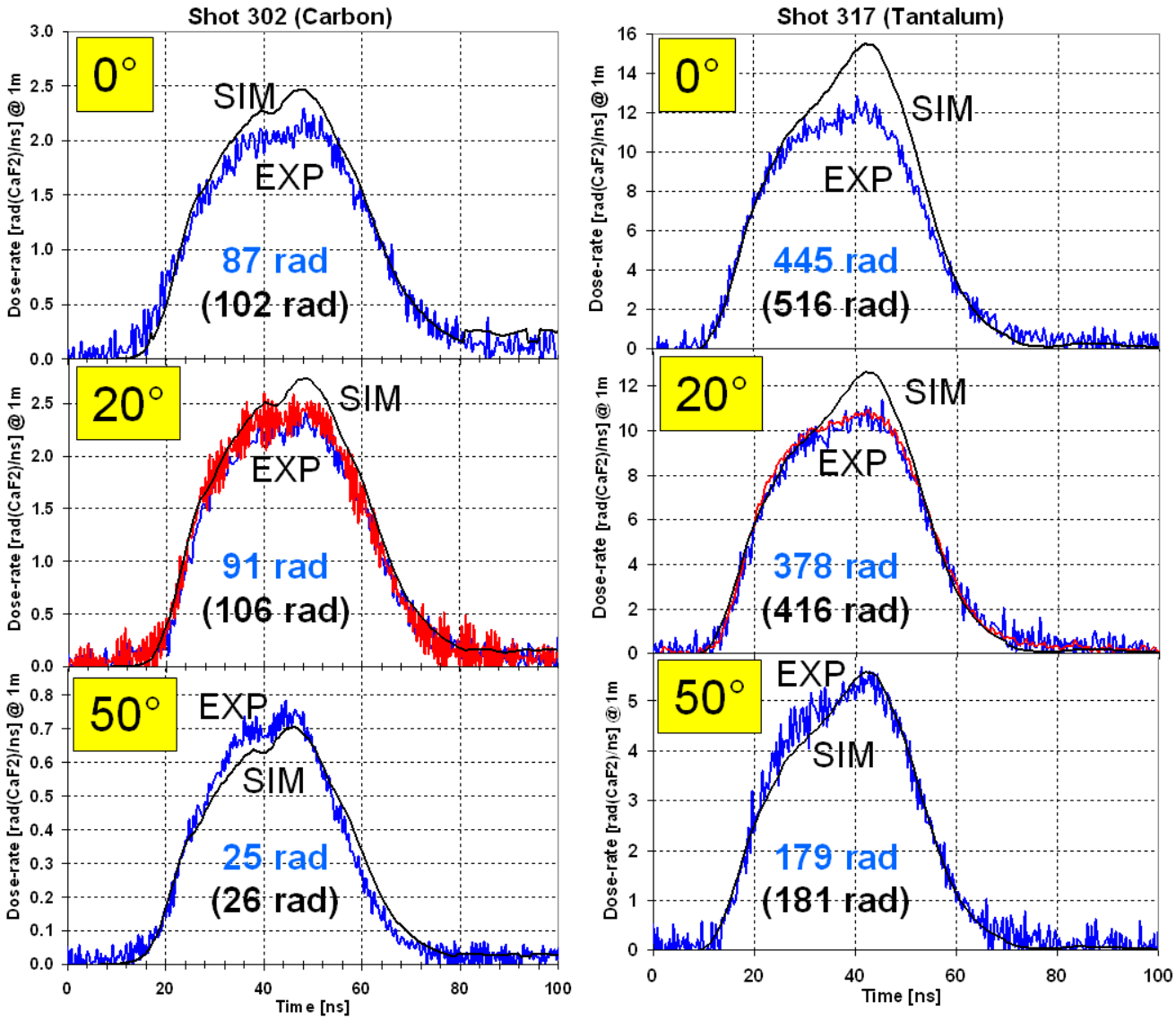

Figure 3. Summary of experimentally fielded and simulated photodiodes at 0°, 20°, and 50°, with left column representing Shot 302 (C) and the right column Shot 317 (Ta). LSP+ITS calculated doses are shown in parentheses.

sources," J. Appl. Phys., vol. 91, pp. 3328 - 3335, Mar. 2002.

[4] J.A. Halbleib, et al., "ITS: the integrated TIGER series of electron/photon transport codes-version 3.0," IEEE Trans. Nucl. Sci. vol. 41, pp. 1025 - 1030, Aug. 1992.

[5] S.B. Swanekamp, et al., "Evaluation of Self-Magnetically Pinched Diodes up to 10 MV as High-Resolution Flash X-ray Sources," IEEE Trans. Plasma Sci. vol. 32, pp. 2004 – 2016, Oct. 2004.

[6] S.B. Swanekamp, et al. "Angular Dose Variations from 4-6 MV Rod-Pinch Experiments on the Asterix Pulsed-Power Generator," in Proc. 14th IEEE International Pulsed Power Conference (Dallas, TX, June 2003), p. 483.

[7] P.F. Ottinger, et al. "Modeling Magnetic Insulated Power Flow in Mercury," in Proc. 14th IEEE International Pulsed Power Conference, (Dallas, TX, June 2003), p. 849.

[8] C.W. Mendel, et al., "Dynamics modeling of magnetically insulated transmission lines systems," Phys. Plasmas, vol. 2, pp. 4207-4219, 1996.

[9] J.H. Hubbell and S.M. Seltzer, Tables of X-Ray Mass Attenuation and Mass Energy-Absorption Coefficients, http://physics.nist.gov/PhysRefData, 1996.